

Electrosynthesis of Atomically Precise Au Nanoclusters

Jing Dong, Yawei Li, Yu Ding, Hai-Feng Su, Xiaoqin Cui, Yu-Xin Wang, and Huan Li*

Innovation in synthesis methodologies is crucial for advancing the discovery of new materials. This work reports the electrosynthesis of a $[\text{Au}_{13}(4\text{-}^t\text{BuPhC}\equiv\text{C})_2(\text{Dppe})_5]\text{Cl}_3$ nanocluster (Au_{13} NC) protected by alkynyl and phosphine ligands. From simple precursor, HAuCl_4 and ligands, the whole synthesis is driven by a constant potential in single electrolytic cell. X-ray crystallography determines its total structure. Control experiments, cyclic voltammetry, Proton Nuclear Magnetic Resonance (^1H NMR), gas chromatography, and other characterizations demonstrate that a critical tetranuclear $\text{Au}(\text{I})$ complex defines the electrochemical redox behavior of the reaction solution. The critical role of a base (e.g., triethylamine) is to suppress the hydrogen evolution reaction at the cathode, paving the way for the reduction of Au ions. To resolve the problem of over-reduction and deposition of Au on the cathode, pulsed electrolysis, which is specific to electrosynthesis is employed. It significantly improves the reaction rate and the isolated yield of Au_{13} . To extend the application scope, another four NCs protected by different ligands, $[\text{Au}_{13}(4\text{-FPhC}\equiv\text{C})_2(\text{Dppe})_5]\text{Cl}_3$, $[\text{Au}_8(2\text{-CF}_3\text{PhC}\equiv\text{C})_2(\text{Dppp})_4](\text{PF}_6)_2$, $[\text{Au}_{11}(\text{Dppp})_5]\text{Cl}_3$, and $[\text{Au}_8(\text{SC}_2\text{H}_4\text{Ph})_2(\text{Dppp})_4]\text{Cl}_2$ are synthesized electrochemically, demonstrating the versatility of the strategy.

potential can be precisely tuned to adjust the reaction rate and selectivity. The merges of electrochemistry with organocatalysis, flow technique, and biochemistry open an even broader application prospect. Thanks to the advantages, recent decades have witnessed an ongoing renaissance of the field. A wide range of organic compounds that would otherwise be difficult to obtain have been electrochemically synthesized.^[3–14] For metal-based materials, electrosynthesis has also proved to be a reliable and versatile strategy. A plethora of metal nanoparticles (nanoclusters),^[15–18] alloy structures,^[19,20] metal oxides,^[21,22] and semiconductors^[23,24] with various sizes and morphologies have been fabricated. Taking gold as example, the wafer-size foil,^[25] nanopore arrays,^[26] nanowire,^[27] and nanoparticles^[28,29] can all be acquired by electrochemical method. Abundant results have convincingly demonstrated the capability of electrosynthesis in a controllable manner at the nanoscale. Transmission Electron Microscope (TEM), Atomic Force Microscope (AFM),

Electrospray Ionization Mass Spectrometry (ESI-MS), and other techniques that have subnanometer to nanometer resolution are usually adequate for their morphology and composition characterization.^[30] Electrochemical methods have been proven to be effective for metal nanoclusters synthesis.^[31,32] Till now, however, single crystals of Au nanoclusters via electrosynthesis have not been isolated yet.

Au nanoclusters (NCs) keep attracting the community's attention owing to their unique physicochemical properties, such as multiple absorption bands, distinct photoluminescence, and well-defined catalytic sites.^[33–38] To gain a fundamental insight into their structure–property relationship, ligand-protected Au NCs whose structures can be determined by single crystal X-ray diffraction are regarded as ideal research models, because their metal cores, peripheral ligands, and stacking modes can all be precisely mapped out. To synthesize them, chemists have mostly relied on solution phase synthesis using a reducing agent (typically, NaBH_4). The method has given birth to a wealth of Au NCs with different nuclearities and ligands.^[39–48] The well-researched Au_{25} NC, for example, was afforded by reducing HAuCl_4 with NaBH_4 under the protection of a 2-phenylethanethiol ligand.^[49] The discoveries of other brilliant methods, such as photochemical method,^[50,51] solid-state synthesis,^[52] etc., have not only provided alternative pathways toward NC, but also shed new light on the formation mechanism.^[53–56]

1. Introduction

Electrosynthesis uses electrical energy to drive chemical reactions, avoiding using some harsh oxidizing and reducing reagents.^[1,2] The magnitude and waveform of the electrical

J. Dong, X. Cui, Y.-X. Wang, H. Li
Institute of Crystalline Materials
Shanxi University
Taiyuan, Shanxi 030006, China
E-mail: 59584340@sxu.edu.cn

Y. Li, Y. Ding
School of Chemistry and Chemical Engineering
Shanxi University
Taiyuan, Shanxi 030006, China
H.-F. Su
Department of Chemistry
College of Chemistry and Chemical Engineering
Xiamen University
Xiamen 361005, P. R. China

 The ORCID identification number(s) for the author(s) of this article can be found under <https://doi.org/10.1002/advs.202414057>

© 2025 The Author(s). Advanced Science published by Wiley-VCH GmbH. This is an open access article under the terms of the [Creative Commons Attribution](#) License, which permits use, distribution and reproduction in any medium, provided the original work is properly cited.

DOI: 10.1002/advs.202414057

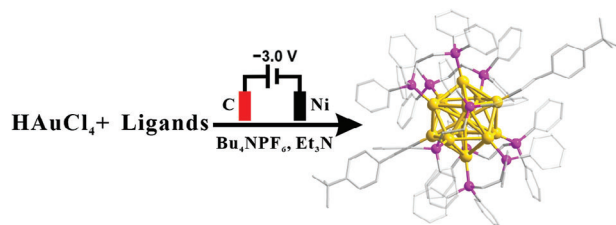


Figure 1. Illustration of the electrosynthesis of $[\text{Au}_{13}(4\text{-}^t\text{BuPhC}\equiv\text{C})_2(\text{Dppe})_5]\text{Cl}_3$ (Au_{13}). Ligands: 4-*tert*-butylphenylacetylene (TBA) and 1,2-bis-(diphenylphosphino)ethane (Dppe). Anode: graphite. Cathode: Ni electrode. Color code: yellow, Au; pink, P; gray, C.

In this work, an Au NC with atomic precision is synthesized in an electrolytic cell for the first time. From a simple precursor, HAuCl_4 to a sophisticated $[\text{Au}_{13}(4\text{-}^t\text{BuPhC}\equiv\text{C})_2(\text{Dppe})_5]\text{Cl}_3$ (Au_{13}), the whole synthesis is driven by a constant potential. The electrochemical redox behavior study, the capture of a critical tetranuclear Au(I) intermediate and the elucidation of the role of amine help to clarify the formation mechanism of Au_{13} under electrochemical conditions. To resolve the problem of over-reduction and deposition of Au on the cathode, pulsed electrolysis is employed, which significantly improves the reaction rate and the isolated yield. To expand the application scope of the strategy, another four Au NCs protected by different ligands including $[\text{Au}_{13}(4\text{-FPhC}\equiv\text{C})_2(\text{Dppe})_5]\text{Cl}_3$, $[\text{Au}_8(\text{SC}_2\text{H}_4\text{Ph})_2(\text{Dppp})_4]\text{Cl}_2$, $[\text{Au}_{11}(\text{Dppp})_5]\text{Cl}_3$, $[\text{Au}_8(2\text{-CF}_3\text{PhC}\equiv\text{C})_2(\text{Dppp})_4](\text{PF}_6)_2$ are also successfully synthesized.

2. Results and Discussion

2.1. Electrosynthesis of Au_{13} Nanocluster

The electrosynthesis of Au_{13} was conducted in a single electrolytic cell where a graphite electrode ($\phi 0.6 \times 0.75$ cm) served as anode (Figure 1). Various materials were evaluated for the cathode, including glassy carbon, Ni, Pt, and graphite electrodes, etc. Based on cost-effectiveness and practical results, Ni plate was employed in most cases. HAuCl_4 , dimethyl sulfide (Me_2S) and the ligands (4-*tert*-butylphenylacetylene (TBA) and 1,2-bis-(diphenylphosphino)ethane (Dppe)) were successively dissolved in a mixture of dichloromethane and ethanol, followed by the addition of triethylamine (Et_3N). Me_2S was employed reduce Au^{3+} to Au^+ , which a common procedure in the synthesis of Au NCs.^[41,47] Tetrabutylammonium hexafluorophosphate (Bu_4NPF_6 , 0.1 M) was employed to increase the conductivity (Figure 1). After a constant potential of -3 V was applied, the color of the solution gradually changed from colorless to brown-red in a few hours (Figures S1 and S2, Supporting Information). The resulting dark transparent solution was centrifuged and concentrated for the following layering process, which yielded red block-shaped crystals in a week. The single crystal was then subjected to characterization by X-ray diffraction. Notably, further aging the as-prepared reaction solution did not result in deterioration, indicating the acceptable stability of Au_{13} under reaction conditions (Figures S3 and S4, Supporting Information). Furthermore, the elemental analysis unveiled negligible Ni^{2+} ions in the resulting solution, likely due to the fact that the Ni electrode, operating as the cathode, exhibited a much reduced tendency to dissolve.

The crystal structure of Au_{13} is shown in Figure 2a. It has a centered icosahedron core composed of thirteen Au atoms (Figure 2b). Two alkynyl ligands are σ -coordinated with Au of the two diagonal apexes of the icosahedron (Figure 2a). Five Dppe form a donut-like belt covering the rest of the surface of the icosahedron (Figure 2c). The ESI mass spectrum of Au_{13} gives a set of signals at around m/z 1622.37, agreeing with the calculated isotope pattern (Figure 2d). The presence of Cl^- counterions in the structure was also confirmed by ion chromatography (Figure S5, Supporting Information). According to the superatom theory, Au_{13} has 8 free valence electrons ($13_{\text{Au}} - 2_{\text{alkyne}} - 3_{\text{Cl}} = 8e$), the same with the previously reported Au_{13} NCs mediated by NaBH_4 (Figure S6, Supporting Information).^[57] On the other side, the weakening of the stretching mode of $\nu(\text{C}\equiv\text{H})$ at 3300 cm^{-1} in the infrared spectrum (IR) of Au_{13} indicates the bonding of TBA with Au (Figure S7, Supporting Information). The UV-vis spectrum of Au_{13} shows absorptions at 314, 446, and 545 nm (Figure 2e).^[57] The optical bandgap is calculated to be 1.49 eV (Figure S8, Supporting Information).^[58] The solution of Au_{13} was also analyzed by square wave voltammetry (SWV, Figure S9, Supporting Information), from which the Highest Occupied Molecular Orbital - Lowest Unoccupied Molecular Orbital gap (HOMO-LUMO gap) was estimated to be 1.38 eV.^[59,60] Both results are in agreement.

2.2. Synthesis Mechanism Study

Since conventional synthesis of Au_{13} NC required a reducing reagent, it was speculated Au_{13} may form at the cathode which reduced the Au precursor by supplying electrons. In a control experiment, the same reactants were charged into both compartments of a divided cell separated by fiberglass membrane. Au species was reduced only in the cathodic compartment, as expected (Figure 3a, inset). Then, the redox behavior at different feeding stages was studied by cyclic voltammetry (CV). As shown in Figure 3b, the solution of HAuCl_4 shows two reduction peaks at -0.15 and -1.16 V (vs SCE), corresponding to $\text{Au}(\text{III}) \rightarrow \text{Au}(\text{I})$ and $\text{Au}(\text{I}) \rightarrow \text{Au}(0)$ conversions.^[61,62] The addition of Me_2S and TBA did not result in significant change. The situation was completely altered when Dppe was introduced. Neither of the above peaks was observed. A more negative reduction peak at -2.1 V emerged. Such a negative shift may arise from the coordination of Dppe with Au. To verify this, only Dppe was used as ligand. The resulting CV in Figure 3c shows obvious resemblance in terms of both potential and shape of the peak.

Next, to capture the potential Au-Dppe complex that may be responsible for such dramatic change, the reaction solution (before electrolysis) was treated by layering. Colorless single crystals were collected in high yield (Figure S10, Supporting Information). X-ray crystallography determined the crystal structure of this tetranuclear Au(I) complex to be $\text{Au}_4(\text{Dppe})_2\text{Cl}_4$ (Figure 3d). It has two Au atoms being bridged by one Dppe and each Au atom is coordinated with a Cl atom to form $\text{Au}_2(\text{Dppe})\text{Cl}_2$. And $\text{Au}_4(\text{Dppe})_2\text{Cl}_4$ is composed of two $\text{Au}_2(\text{Dppe})\text{Cl}_2$ parts, forming a centrosymmetric dimer through aurophilic interaction.^[63] The same solution that afforded $\text{Au}_4(\text{Dppe})_2\text{Cl}_4$ was also dried and subjected to powder XRD analysis (Figure 3e). The resulting pattern fits the simulation result from the crystal structure

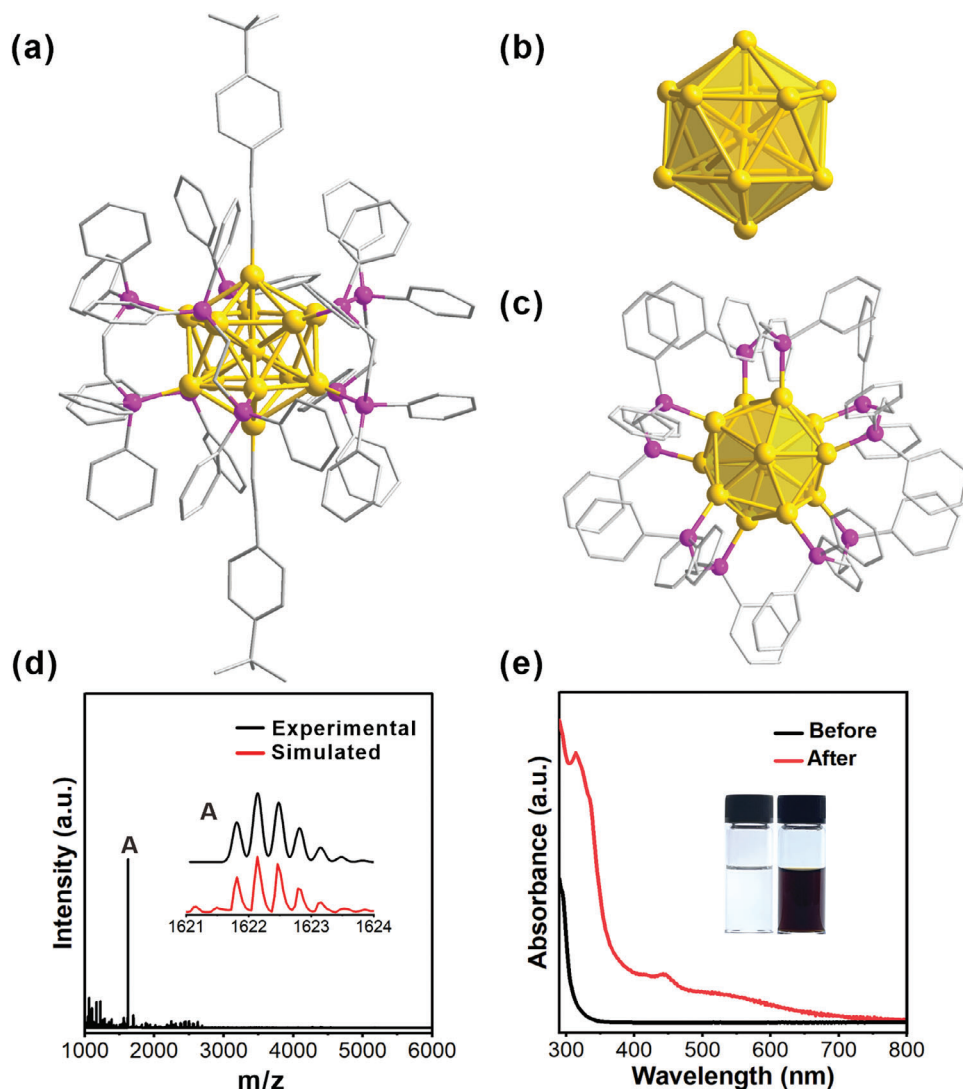


Figure 2. Total structure a) and core structure b) of Au_{13} . c) Distribution and coordination patterns of phosphine ligands. d) Mass spectrum of Au_{13} . Inset: experimental (black trace) and simulated (red trace) isotopic patterns of the molecular ion peak for $[\text{Au}_{13}(4\text{-}^t\text{BuPhC}\equiv\text{CR})_2(\text{Dppe})_5]\text{Cl}_3$. e) UV-vis absorption spectra of the Au_{13} solution before (black line) and after 12 h electrolysis (red line). The inset is photographs of the vessel before (left) and after (right) electrolysis.

of $\text{Au}_4(\text{Dppe})_2\text{Cl}_4$. This means that $\text{Au}_4(\text{Dppe})_2\text{Cl}_4$ is likely the dominant Au related species in solution, which dictates its redox behavior. Because the peak potential was -2.1 V. To ensure that the cathodic reduction occurred, a more negative potential was required. Although the reaction proceeded at -2.5 V, the progress was sluggish. In practice, a potential of -3 V was applied effectively (Figures S11 and S12, Supporting Information).

During the course of electrosynthesis, the reaction solution was subjected to CV analysis at intervals. The combined results in Figure S13 (Supporting Information) show that the reduction peak current (i_p) gradually decreased, indicating $\text{Au}_4(\text{Dppe})_2\text{Cl}_4$ was slowly consumed as the reaction went on. Eventually, the peak at -2.1 V disappeared, and the solution turned brown red. The CV curve, however, shows no corresponding oxidation peak in anodic scan, implying an irreversible electrode reaction (Figure 3c). To confirm that, CV scans at varying rates

were conducted ($30\text{--}250$ mV s^{-1} , Figure S14, Supporting Information). The results showed a linear relationship between peak potential E_p and $\log v$ (v is scan rate), meeting the Laviron equation (Figure S15, Supporting Information).^[64] Additionally, the reduction peak current I_p plotted against $v^{1/2}$ followed the Randles-Sevcik equation,^[65,66] indicating diffusion-limited kinetics (Figure S16, Supporting Information).

When ligands were not present, Au ions still got reduced, but the products were black precipitate (Au nanoparticles). When only alkyne was used as ligand, no stable NC colloidal solution was formed and cathode deposition of Au was evident. The reaction progress was sluggish when using only Dppe as ligand (Figure 4a). No single crystal of Au NC was collected after work-up in both cases. To explore the difference between the traditional and electrosynthesis, NaBH_4 was employed using the same recipe without applying electric potential. The colors of the

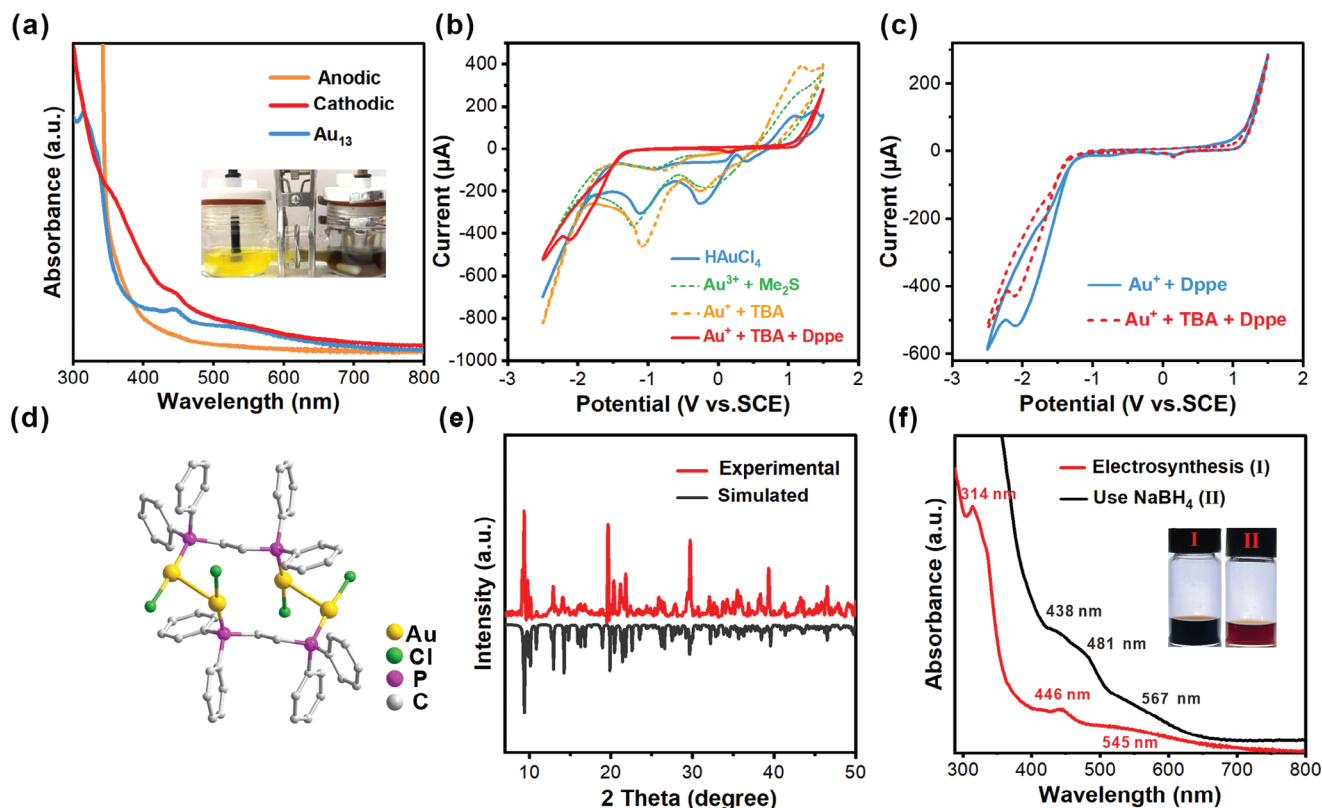


Figure 3. a) UV–vis spectra of the solutions from divided cell. The spectrum of Au_{13} is included for comparison. Insert: the photograph of the reaction vessel after 12 h electrosynthesis. The right part of the vessel is the cathodic compartment. b) Cyclic voltammograms (CV) of the solution at different feeding stages (scan rate = 100 mV s^{-1}). Me_2S is dimethyl sulfide, TBA is 4-*tert*-butylphenylacetylene and Dppe is 1,2-bis-(diphenylphosphino)ethane. c) The CV comparison of the solutions containing different components. They show evident resemblance. d) The crystal structure of $\text{Au}_4(\text{Dppe})_2\text{Cl}_4$. e) The powder XRD patterns of the dried reaction solution (before electrolysis, red line) and the one simulated from the single crystal of $\text{Au}_4(\text{Dppe})_2\text{Cl}_4$ (black line). f) UV–vis absorption spectra of Au nanoclusters synthesized by electro-synthesis (red line) and by NaBH_4 (black line).

resulting solutions and the UV–vis absorption spectra showed obvious differences. The one using NaBH_4 showed peaks at 438, 481, and 567 nm, quite different from that by electro-synthesis (Figure 3f). This may indicate different product structures. Through our observation, the reaction solution immediately turned from colorless to brown upon the introduction of NaBH_4 , while for electro-synthesis, the color transition was slow (typically hours before an obvious color change can be observed). The difference in reduction kinetics could be responsible for this, although the precise mechanism requires future thorough investigation. Curiously, without Et_3N , the reaction did not proceed, either (Figure S17a, Supporting Information). To figure it out, different characterizations were performed. ^1H NMR spectrum of the resulting solution shows the same H count and multiplicity as that of Et_3N , although the signals shift to downfield (Figure 4b). This was empirically attributed to protonation of Et_3N (Et_3NH^+). It was then confirmed by the mass spectroscopy by showing a signal at m/z 102.128 (calc. m/z 102.199, Figure 4c). The function of Et_3N was to capture the protons which were likely from HAuCl_4 , 4-*tert*-butylphenylacetylene or protons produced by oxidation of solvents.

The ensuing question is why a relatively acidic environment suppressed the formation of Au_{13} . Our speculation was that H^+ reduction (hydrogen evolution reaction, HER) at the cathode may

be a highly competitive reaction, since the reduction potential of $\text{Au}(\text{I})$ species was more negative than the reduction of H^+ . As shown in the linear sweep voltammetry (LSV, Figure 4d), in the absence of Et_3N , the current of HER became evident at about -0.5 V , significantly more positive than that required for the synthesis of Au_{13} . On the other hand, adding Et_3N greatly suppressed the HER. For example, at -1.5 V , the current density was -8.64 mA cm^{-2} without Et_3N . When Et_3N was increased from 30 to $100 \mu\text{L}$, the current density decreased markedly to -3.77 and -0.99 mA cm^{-2} , respectively. The gas phase of the reaction vessel was also analyzed by gas chromatography equipped with thermal conductivity detector (TCD, Figure 4e). The sharp peak at retention time of 0.33 min was assigned to H_2 . In the absence of Et_3N , H_2 concentration was 12244 ppm. The values dropped to 4567 and 1332 ppm when 30 and $100 \mu\text{L}$ Et_3N were fed, respectively (Figure 4e). HER was effectively inhibited by Et_3N , paving the way for the reduction of Au species. Furthermore, the more amine was used, the faster the reaction went, which is illustrated in Figure S17 (Supporting Information). With this information, we assumed that another base may also be effective. When NaOH was used instead of Et_3N , the same Au_{13} was produced (Figure 4f, inset). Powder XRD of the resulting dried solution showed NaCl was the product, indicating that NaOH was neutralized (Figure 4f). In a separate experiment, when HCl

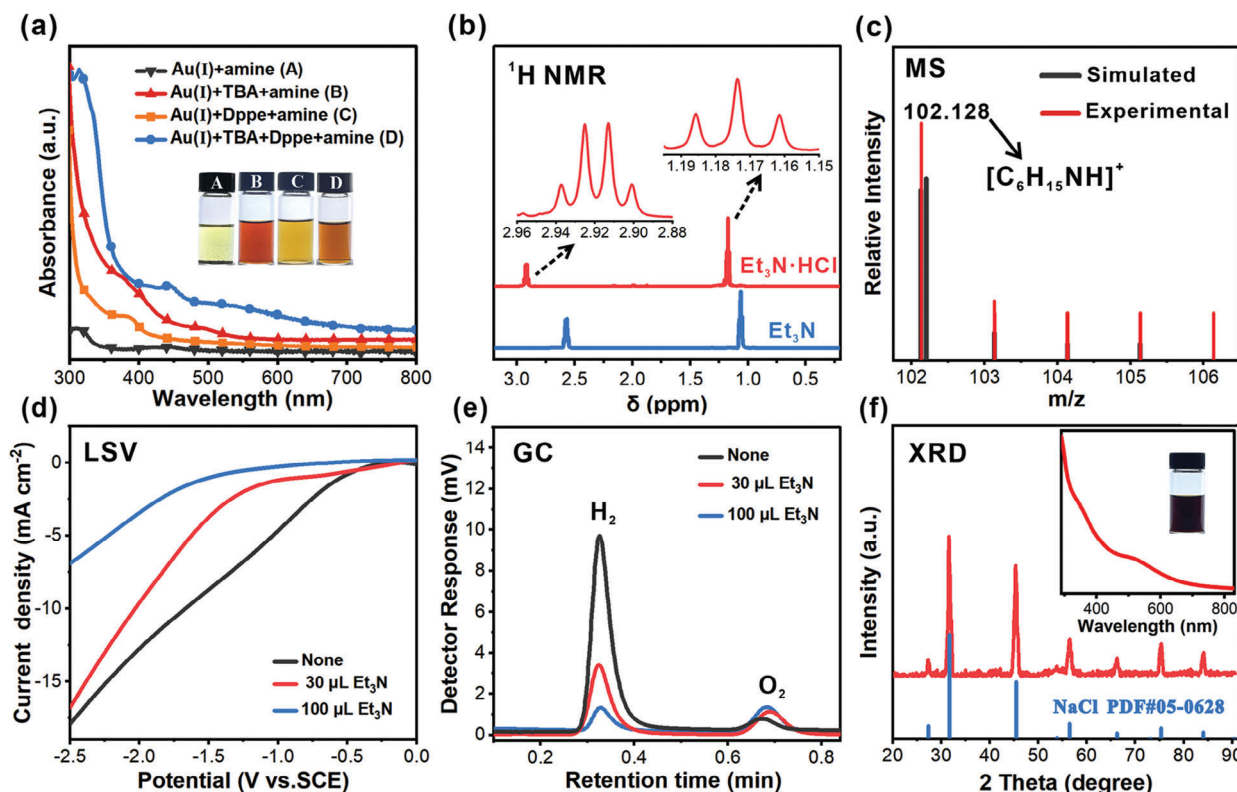


Figure 4. a) UV-vis spectra of the reaction solution after electrolysis with different reactants. Inset: corresponding photographs. b) ^1H NMR spectra of reaction solution after electrosynthesis using HAuCl_4 and Et_3N (red line) and the spectrum of Et_3N (blue line). c) High-resolution mass spectrum of the reaction solution the same as that in (b). d) Linear sweep voltammetry (LSV) curves of reaction solution in the presence of different amounts of Et_3N . Scan rate, $\nu = 5 \text{ mV s}^{-1}$. Working electrode: Ni plate; counter electrode: graphite; reference electrode: saturated calomel electrode. e) Gas chromatography (GC) analysis: the signal response of H_2 during electrosynthesis with different amount of Et_3N . f) XRD pattern of the dried reaction solution using NaOH as a base. Inset: UV-vis spectrum and the photograph of vessel after reaction.

solution was deliberately charged into the vessel during the electrosynthesis of Au_{13} , the formation of Au_{13} ceased. And introducing NaOH restarted the progress (Figure S18, Supporting Information), further confirming our speculation.

2.3. Pulsed Potential Synthesis

Unfortunately, black deposit on the Ni electrode was always seen after electrosynthesis under constant potential. The isolated yield of Au_{13} was relatively low (less than 13%, Figure 5a, (I)). X-ray diffraction pattern of the used Ni electrode showed an X-ray diffraction peak at 38.2° , resulting from the face-centered cubic Au (111) plane. A portion of Au(I) was reduced to Au nanoparticles (Figure 5d, (I)). Also, after rinsing the used Ni-electrode with CH_2Cl_2 , the collected solution showed similar characteristic absorptions with that of Au_{13} (Figure 5e, (I)). These results indicated under constant potential, Au(I) species tended to be over reduced and deposited on the electrode. To alleviate the problem, we resorted to pulsed potential electrolysis, which occasionally showed dramatic effect in organic electrosynthesis.^[67,68] To our delight, this technique turned out to be very effective. When the pulse width was set to 60 s, (on for 60 s, off for 60 s), the reaction proceeded obviously faster (Figure S19, Supporting Information), and the isolated yield of Au_{13} increased to an average of 28%

(Figure 5b, (II)). Shortening the pulse width to 10 s further accelerated the reaction. Even more Au_{13} crystals were collected after workup (isolated yield up to 36%, Figure 5c, (III)). Further shortening of the pulse interval did not result in significant changes. Both the XRD patterns and spectral features showed no sign of over-reduction or NC deposition (Figures 5d,e). It is deduced that the Au(0) species deposited on the cathode may inhibit the continuous reduction of Au(I) species under constant potential. The pulsed potential allows the reduced species to leave the cathodic region to avoid over-reduction. Although the underlying mechanism is yet to be fully verified, simply adjusting the potential waveform can increase the yield of Au NCs, demonstrating the technical advantage of electrosynthesis that is difficult to achieve through conventional synthesis methods.

2.4. Application Scope of Electrosynthesis

If electrolytic cell is to be qualified as a new platform for exploiting novel NCs with atomic precision, a good range of applicability is a critical criterion. For that, different ligands were screened (Figures S20 and S21, Supporting Information). Replacing TBA with 4-fluorophenylacetylene while keeping the other conditions the same yielded a $[\text{Au}_{13}(\text{4-FPhC}\equiv\text{C})_2(\text{Dppe})_5]\text{Cl}_3$ NC ($\text{Au}_{13}\text{-2}$) (Figure 6a). Despite the difference in alkynyl ligand,

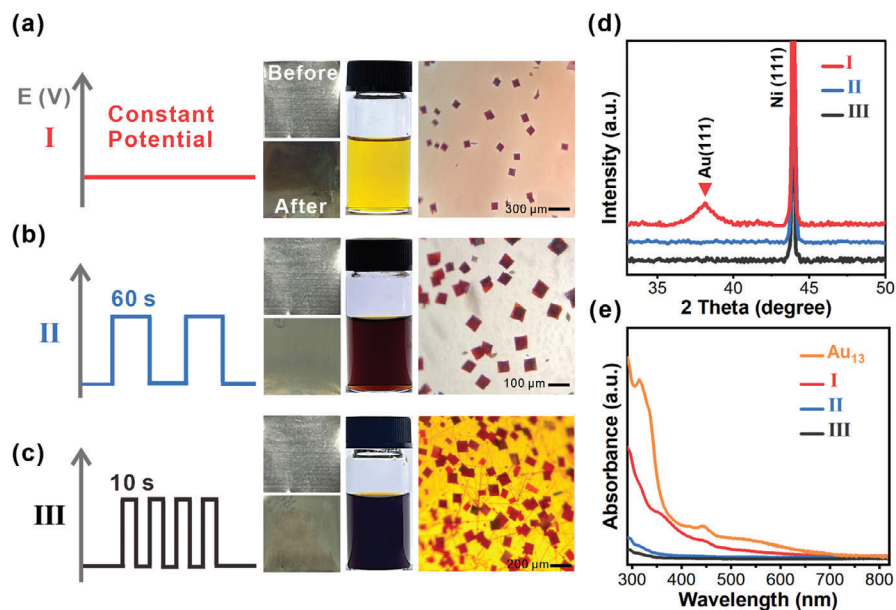


Figure 5. a) (I) represents the results obtained under constant potential. The photo on the left is the Ni electrode before and after electrosynthesis. The one in the middle is the reaction vessel after 4 h of electrosynthesis. The one on the right is the single crystal of Au_{13} . (b) and (c) are corresponding results under pulsed potentials. Pulse width is 60 s for (II) and 10 seconds for (III). d) XRD patterns of the used Ni electrodes. e) UV-vis spectra of the solutions formed by rinsing the used Ni electrodes with CH_2Cl_2 .

Scope of Electrosynthesis of Au Nanoclusters

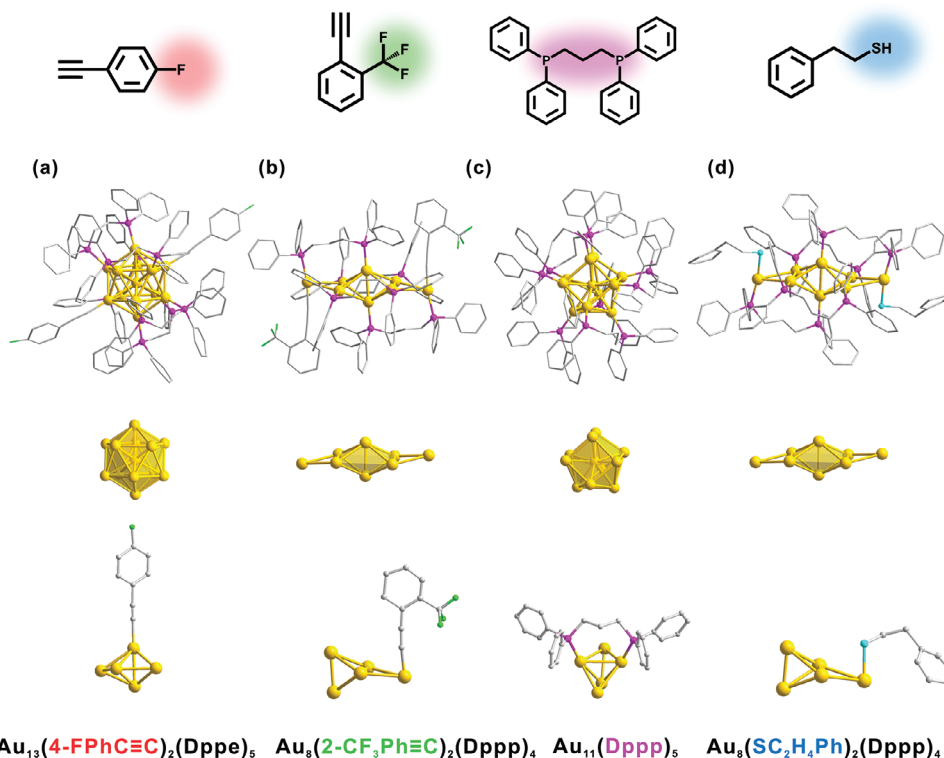


Figure 6. Scope of application. The structure anatomy of $[\text{Au}_{13}(\text{4-FPhC}\equiv\text{C})_2(\text{Dppe})_5]\text{Cl}_3$ (**Au₁₃-2**) a). $[\text{Au}_8(\text{2-CF}_3\text{PhC}\equiv\text{C})_2(\text{Dppp})_4](\text{PF}_6)_2$ (**Au₈-1**) b). $[\text{Au}_{11}(\text{Dppp})_5]\text{Cl}_3$ (**Au₁₁**) (c) and $[\text{Au}_8(\text{SC}_2\text{H}_4\text{Ph})_2(\text{Dppp})_4]\text{Cl}_2$ (**Au₈-2**) d). Color code: yellow, Au; pink, P; gray, C; green, F; blue, S. All hydrogen atoms are omitted for clarity.

its overall structure was similar with that of Au_{13} . ESI mass analysis shows an intense peak at m/z 1596.76, which is assigned to the $[\text{Au}_{13}(\text{4-FPhC}\equiv\text{C})_2(\text{Dppe})_5]^{3+}$ NC (Figure S22a, Supporting Information). The unity spacing of the isotopes indicates that the $[\text{Au}_{13}(\text{4-FPhC}\equiv\text{C})_2(\text{Dppe})_5]^{3+}$ NC ion bears three charges. A combination of 1,3-bis(diphenylphosphino)propane (Dppp) and 2-(trifluoromethyl)phenylacetylene gave birth to a $[\text{Au}_8(\text{2-CF}_3\text{PhC}\equiv\text{C})_2(\text{Dppp})_4](\text{PF}_6)_2$ NC (**Au₈-1**) (Figures 6b; and S23, Supporting Information). The core of **Au₈** consists of an Au_6 octahedral core and two extended gold atoms, each of which accommodates one phosphine and one alkynyl group (Figure 6b).^[69] By reducing the amount of alkynyl ligands, an all-phosphine-protected $[\text{Au}_{11}(\text{Dppp})_5]\text{Cl}_3$ NC (**Au₁₁**) was synthesized (Figure 6c). **Au₁₁** core can be described as a central gold atom surrounded by an icosahedron in which one triangle was replaced by a Au atom.^[70] Furthermore, thiolate has been more widely used than alkynyl for Au NCs. To test whether electrosynthesis is suitable for thiolate ligand, 2-phenylethanethiol was used in place of alkynyl. A $[\text{Au}_8(\text{SC}_2\text{H}_4\text{Ph})_2(\text{Dppp})_4]\text{Cl}_2$ NC (**Au₈-2**) NC was acquired (Figure 6d). The difference between **Au₈-2** and **Au₈-1** is that the extended Au atom of **Au₈-2** coordinates with a thiolate ligand other than alkynyl ligand.^[71] The mass peaks of $[\text{Au}_8(\text{2-CF}_3\text{PhC}\equiv\text{C})_2(\text{Dppp})_4]^{2+}$, $[\text{Au}_{11}(\text{Dppp})_5]^{3+}$, and $[\text{Au}_8(\text{SC}_2\text{H}_4\text{Ph})_2(\text{Dppp})_4]^{2+}$ are observed at m/z 1781.72, 1409.48, and 1749.83, respectively (theoretical values: 1781.67, 1409.46, and 1749.72), as shown in Figures S22b and S22c (Supporting Information). They agree with the calculated isotopic patterns.

3. Conclusion

An electrochemical platform for synthesizing Au nanoclusters with atomic precision is established. The technical features, underlying mechanism, and scope of application are investigated. A tetranuclear intermediate $\text{Au}(\text{I})$ complex defines the redox behavior of the reaction solution. The critical role of base is to suppress the hydrogen evolution reaction at the cathode. By employing pulsed potential, the reaction rate and the yield of Au nanoclusters are significantly improved. The study aims to pushing the electrosynthesis to atom-precision and inspiring future synthesis of various metal nanoclusters by this strategy.

Supporting Information

Supporting Information is available from the Wiley Online Library or from the author.

Acknowledgements

This work was supported by the National Natural Science Foundation of China (Nos. 21972080 and 21503123), Natural Science Research Foundation of Shanxi Province (No. 202303021221060).

Conflict of Interest

The authors declare no conflict of interest.

Data Availability Statement

The data that support the findings of this study are available in the Supporting Information of this article.

Keywords

Au nanoclusters, electrosynthesis, pulsed electrolysis

Received: November 14, 2024
Revised: February 15, 2025
Published online: March 13, 2025

- [1] M. C. Leech, K. Lam, *Nat. Rev. Chem.* **2022**, 6, 275.
- [2] C. Kingston, M. D. Palkowitz, Y. Takahira, J. C. Vantourout, B. K. Peters, Y. Kawamata, P. S. Baran, *Acc. Chem. Res.* **2020**, 53, 72.
- [3] M. Rafiee, D. J. Abrams, L. Cardinale, Z. Goss, A. Romero-Arenas, S. S. Stahl, *Chem. Soc. Rev.* **2024**, 5, 566.
- [4] L. F. T. Novaes, J. Liu, Y. Shen, L. Lu, J. M. Meinhardt, S. Lin, *Chem. Soc. Rev.* **2021**, 50, 7941.
- [5] Y. Wang, S. Dana, H. Long, Y. Xu, Y. Li, N. Kaplaneris, L. Ackermann, *Chem. Rev.* **2023**, 123, 11269.
- [6] Y. H. Budnikova, E. L. Dolengovski, M. V. Tarasov, T. V. Gryaznova, *J. Solid State Electrochem.* **2023**, 28, 659.
- [7] C. Zhu, N. W. J. Ang, T. H. Meyer, Y. Qiu, L. Ackermann, *ACS Cent. Sci.* **2021**, 7, 415.
- [8] Y. Hioki, M. Costantini, J. Griffin, K. C. Harper, M. P. Merini, B. Nissl, Y. Kawamata, P. S. Baran, *Science* **2023**, 380, 81.
- [9] D. Lehnher, L. Chen, *Org. Process Res. Dev.* **2024**, 28, 338.
- [10] T. H. Meyer, I. Choi, C. Tian, L. Ackermann, *Chem* **2020**, 6, 2484.
- [11] L. Zeng, Q. Yang, J. Wang, X. Wang, P. Wang, S. Wang, S. Lv, S. Muhammad, Y. Liu, H. Yi, A. Lei, *Science* **2024**, 38, 216.
- [12] Y. Yuan, J. Yang, A. Lei, *Chem. Soc. Rev.* **2021**, 50, 10058.
- [13] M. Yan, Y. Kawamata, P. S. Baran, *Chem. Rev.* **2017**, 117, 13230.
- [14] N. Wang, S. Ma, P. Zuo, J. Duan, B. Hou, *Adv. Sci.* **2021**, 8, 2100076.
- [15] I. Saldan, O. Dobrovetska, L. Sus, O. Makota, O. Pereviznyk, O. Kuntzi, O. Reshetnyak, *J. Solid State Electrochem.* **2018**, 22, 637.
- [16] J. Hong, X. Su, *J. Am. Chem. Soc.* **2024**, 146, 18586.
- [17] N. Tian, Z.-Y. Zhou, S.-G. Sun, Y. Ding, Z. L. Wang, *Science* **2007**, 316, 732.
- [18] L. Zhao, Y. Wang, S. Jin, N. An, M. Yan, X. Zhang, Z. Hong, S. Yang, *Nat. Synth.* **2024**, 3, 867.
- [19] M. W. Glasscott, A. D. Pendergast, S. Goines, A. R. Bishop, A. T. Hoang, C. Renault, J. E. Dick, *Nat. Commun.* **2019**, 10, 2650.
- [20] S. Butcha, S. Assavapanumat, S. Ittisanronnachai, V. Lapeyre, C. Wattanakit, A. Kuhn, *Nat. Commun.* **2021**, 12, 1314.
- [21] D. Ramimoghaddam, S. Bagheri, S. B. A. Hamid, *J. Magn. Mater.* **2014**, 368, 207.
- [22] N. An, T. Chen, J. Zhang, G. Wang, M. Yan, S. Yang, *Small Methods* **2024**, 8, 2300910.
- [23] S. Cestellos-Blanco, H. Zhang, J. M. Kim, Y. Shen, P. Yang, *Nat. Catal.* **2020**, 3, 245.
- [24] K. Rajeshwar, A. Vali, A. Rawat, N. Myung, *Acc. Chem. Res.* **2023**, 56, 994.
- [25] N. K. Mahenderkar, Q. Chen, Y.-C. Liu, A. R. Duchild, S. Hofheins, E. Chason, J. A. Switzer, *Science* **2017**, 35, 1203.
- [26] H. Masuda, K. Fukuda, *Science* **1995**, 268, 1466.
- [27] H. Yao, J. Duan, D. Mo, H. Yusuf Günel, Y. Chen, J. Liu, T. Schäpers, *J. Appl. Phys.* **2011**, 11, 094301.
- [28] M. A. Saucedo-Espinosa, M. Breitfeld, P. S. Dittrich, *Angew. Chem., Int. Ed.* **2023**, 6, e202212459.

- [29] L. Zhang, R. Hao, D. Zhang, H. You, Y. Dai, W. Liu, J. Fang, *Anal. Chem.* **2020**, 92, 9838.
- [30] M. M. Modena, B. Rühle, T. P. Burg, S. Wuttke, *Adv. Mater.* **2019**, 31, 1901556.
- [31] B. S. González, M. J. Rodríguez, C. Blanco, J. Rivas, M. A. López-Quintela, J. M. Gaspar Martinho, *Nano Lett.* **2010**, 10, 4217.
- [32] B. S. González, M. C. Blanco, M. A. López-Quintela, *Nanoscale* **2012**, 4, 7632.
- [33] J. Kong, W. Zhang, Y. Wu, M. Zhou, *Aggregate* **2022**, 3, e207.
- [34] J. Olesiak-Banska, M. Waszkielewicz, P. Obstarczyk, M. Samoc, *Chem. Soc. Rev.* **2019**, 48, 4087.
- [35] Z. Liu, L. Luo, R. Jin, *Adv. Mater.* **2024**, 36, 2309073.
- [36] X. Cai, G. Li, W. Hu, Y. Zhu, *ACS Catal.* **2022**, 12, 10638.
- [37] Z. Guan, J. Li, F. Hu, Q. Wang, *Angew. Chem., Int. Ed.* **2022**, 61, e202209725.
- [38] R. H. Adnan, J. M. L. Madridejos, A. S. Alotabi, G. F. Metha, G. G. Andersson, *Adv. Sci.* **2022**, 9, 2105692.
- [39] F. Gao, Q. Yuan, P. Cai, L. Gao, L. Zhao, M. Liu, Y. Yao, Z. Chai, X. Gao, *Adv. Sci.* **2019**, 6, 1801671.
- [40] H. Zhao, C. Zhang, B. Han, Z. Wang, Y. Liu, Q. Xue, C.-H. Tung, D. Sun, *Nat. Synth.* **2024**, 3, 517.
- [41] X. Kang, H. Chong, M. Zhu, *Nanoscale* **2018**, 10, 10758.
- [42] S. Kenzler, A. Schnepf, *Chem. Sci.* **2021**, 1, 3116.
- [43] N. Xia, Z. Wu, *Chem. Sci.* **2021**, 12, 2368.
- [44] C. Zeng, Y. Chen, K. Kirschbaum, K. Appavoo, M. Y. Sfeir, R. Jin, *Sci. Adv.* **2015**, 1, e1500045.
- [45] B. Santiago-Gonzalez, A. Monguzzi, J. M. Azpiroz, M. Prato, S. Erratico, M. Campione, R. Lorenzi, J. Pedrini, C. Santambrogio, Y. Torrente, F. De Angelis, F. Meinardi, S. Brovelli, *Science* **2016**, 353, 571.
- [46] C. Sun, B. K. Teo, C. Deng, J. Lin, G.-G. Luo, C.-H. Tung, D. Sun, *Coord. Chem. Rev.* **2021**, 427, 213576.
- [47] B. Zhang, J. Chen, Y. Cao, O. J. H. Chai, J. Xie, *Small* **2021**, 17, 2004381.
- [48] L. Wang, J. Du, J. Wu, Z. A. Nan, S. Li, X. Tang, Z. Xie, Q. Xu, X. Gong, J. He, R. Chen, H. Shen, *Adv. Sci.* **2024**, 12, 2410796.
- [49] M. Zhu, E. Lanni, N. Garg, M. E. Bier, R. Jin, *J. Am. Chem. Soc.* **2008**, 130, 1138.
- [50] Y.-X. Wang, J. Zhang, H.-F. Su, X. Cui, C.-Y. Wei, H. Li, X.-M. Zhang, *ACS Nano* **2023**, 17, 11607.
- [51] Z.-M. Zhu, Y. Zhao, H. Zhao, C. Liu, Y. Zhang, W. Fei, H. Bi, M.-B. Li, *Nano Lett.* **2023**, 23, 7508.
- [52] T. U. B. Rao, B. Nataraju, T. Pradeep, *J. Am. Chem. Soc.* **2010**, 132, 16304.
- [53] T. Udayabhaskararao, T. Pradeep, *J. Phys. Chem. Lett.* **2013**, 4, 1553.
- [54] H. Xu, K. S. Suslick, *ACS Nano* **2010**, 4, 3209.
- [55] I. Chakraborty, T. Udayabhaskararao, G. K. Deepesh, T. Pradeep, *J. Mater. Chem. B* **2013**, 1, 4059.
- [56] S. Antonello, T. Dainese, F. Pan, K. Rissanen, F. Maran, *J. Am. Chem. Soc.* **2017**, 139, 4168.
- [57] M. Suguchi, Y. Shichibu, T. Nakanishi, Y. Hasegawa, K. Konishi, *Chem. Commun.* **2015**, 51, 13519.
- [58] K. Kwak, V. D. Thanthirige, K. Pyo, D. Lee, G. Ramakrishna, *J. Phys. Chem. Lett.* **2017**, 8, 4898.
- [59] M. Kim, Q. Tang, A. V. Narendra Kumar, K. Kwak, W. Choi, D. Jiang, D. Lee, *J. Phys. Chem. Lett.* **2018**, 9, 982.
- [60] K. Kwak, D. Lee, *Acc. Chem. Res.* **2019**, 52, 12.
- [61] U. Koelle, A. Laguna, *Inorg. Chim. Acta* **1999**, 290, 44.
- [62] M. B. Hariri, *Anal. Methods* **2021**, 13, 2688.
- [63] S. Eggleston, F. Chodosh, R. Girard, D. T. Hill, *Inorg. Chim. Acta* **1985**, 108, 221.
- [64] M. Rezaei, S. H. Tabaian, D. F. Haghshenas, *J. Electroanal. Chem.* **2012**, 687, 95.
- [65] C. Su, M. An, P. Yang, H. Gu, X. Guo, *Appl. Surf. Sci.* **2010**, 256, 4888.
- [66] X. Li, H. Su, R. Zhou, S. Feng, Y. Tan, X. Wang, J. Jia, M. Kurmoo, D. Sun, L. Zheng, *Chem.-Eur. J.* **2016**, 22, 3019.
- [67] T. Liu, J. Wang, X. Yang, M. Gong, *J. Energy Chem.* **2021**, 59, 69.
- [68] G. González-Rubio, A. Guerrero-Martínez, L. M. Liz-Marzán, *Acc. Chem. Res.* **2016**, 49, 678.
- [69] N. Kobayashi, Y. Kamei, Y. Shichibu, K. Konishi, *J. Am. Chem. Soc.* **2013**, 135, 16078.
- [70] J. M. M. Smits, J. J. Bour, F. A. Vollenbroek, P. T. Beurskens, *J. Crystallogr. Spectrosc. Res.* **1983**, 13, 355.
- [71] M. Iwasaki, N. Kobayashi, Y. Shichibu, K. Konishi, *Phys. Chem. Chem. Phys.* **2016**, 18, 19433.